Int J Thermophys (2009) 30:1242–1256
DOI 10.1007/s10765-009-0649-4

Investigation of Water Absorption and Diffusion in Microparticles Containing Xylitol to Provide a Cooling Effect by Thermal Analysis

F. Salaün · G. Bedek · E. Devaux · D. Dupont · D. Deranton

Received: 15 October 2008 / Accepted: 27 August 2009 / Published online: 23 September 2009

Abstract Polyurethane microparticles containing xylitol as a sweat sensor system were prepared by interfacial polymerization. The structural and thermal properties of the resultant microparticles were studied. The surface morphology and chemical structure of microparticles were investigated using an optical microscope (OM) and a Fourier-transform infrared spectroscope (FTIR), respectively. The thermal properties of samples were investigated by thermogravimetric analysis (TGA) and by differential scanning calorimetry (DSC). Thus, two types of microparticles were synthesized by varying the percentage of monomers introduced. The obtained morphology is directly related to the synthesis conditions. DSC analysis indicated that the mass content of crystalline xylitol was up to 63.8 %, which resulted in a high enthalpy of dilution of $127.7\,\mathrm{J}\cdot\mathrm{g}^{-1}$. Furthermore, the water release rate monitored by TGA analysis was found to be faster from the microparticles than from raw xylitol. Thus, the microparticles could be applied for thermal energy storage and moisture sensor enhancement.

Keywords Microencapsulation · Thermal properties · Water release · Xylitol

F. Salaün · G. Bedek · E. Devaux
Laboratoire de Génie et Matériaux Textiles (GEMTEX), UPRES EA2461, BP 30329, 59056 Roubaix Cedex 01, France

D. Dupont · D. Deranton
Haute Etudes d'Ingénieur (HEI), 13 rue de Toul, 59046 Lille, France

F. Salaün (✉)
ENSAIT-GEMTEX, 9 rue de l'ermitage, BP 30329, 59100 Roubaix, France
e-mail: fabien.salaun@ensait.fr

1 Introduction

Smart textiles are able to sense electrical, thermal, chemical, magnetic, or other stimuli from the environment and adapt or respond to them, using functionalities integrated into the textile structure. As an important consideration in active wear, clothing comfort is closely related to the microclimate temperature and humidity between clothing and skin. On the one hand, latent heat storage is one of the most efficient way of storing thermal energy in a textile area. Thus, over the last decades, research has been focussed on the use of phase change materials to improve thermal insulation of textile materials during changes in environmental conditions. On the other hand, sweating is one of the primary modes by which humans attempt to lose excess of body heat. Sensible sweating starts to create latent heat flux by evaporating sweat at the skin surface. Increased sweat evaporation increases the relative humidity of the microclimate which can lead to discomfort if adequate vapor transmission is not permitted by the clothing. Thus, thermal equilibrium and comfort are also dependent on moisture permeation of clothing [1].

Among the three kinds of thermal storage, reversible chemical reaction heat storage is the least popular in the thermal comfort area. Thermo-chemical heat storage has numerous advantages, i.e., high energy density, high discharge power due to high reaction enthalpy, wide reaction temperature range, high heat and mass transfer rates, fast reaction kinetic, low material prices, and non-toxic material. A wide variety of substances may result in a temperature change when contacted with an aqueous solution, e.g., crystalline polyols, salt hydrates, and anhydrous salts [2]. The crystalline form of xylitol presents a cooling effect due to its negative heat of solution at 35 °C ($-36.5\,\mathrm{kcal}\cdot\mathrm{kg}^{-1}$) support by humidity absorption, contributing to a fresh sensation when xylitol dissolves [3]. Since this material is sometimes in a liquid state, it cannot be incorporated in or onto a substrate without being protected. One of the strategies to protect the active substance may be formation of a barrier layer at its surface, i.e., microencapsulation [4–7].

For the case when materials are sensitive to moisture, a step of encapsulation with a semi-impermeable coating is necessary to improve their thermal performance [8–10]. The functional performance of the microparticles depends on the morphology, chemical nature, and surface characteristics of the polymeric shell influenced by the process parameters [8]. The choice of a particular process is determined by the solubility characteristics of the active compound and the shell material. Among the variety of polycondensates possible, polyurethane–urea seems to be of particular interest with widespread characteristics by molecular composition [11–15]. In a water-in-oil polycondensation system to prepare a polyurethane network, it is known that the reaction of isocyanate groups with water molecules during the capsule formation also forms urea cross-linkings. This formation depends on water molecule diffusion through the polyurethane network and could influence the thermal properties controlling the permeation properties of the microparticles. The release rate of the active agent from the microparticles can also be influenced by the chemical nature of the shell, its thickness, and the mean diameter [16].

The aim of this study is to evaluate the thermal properties of microencapsulated xylitol. A two-step microencapsulation process has been applied to obtain the

microparticles. The first step is liquid–liquid dispersion, and the second step is microencapsulation by interfacial polymerization. The process can be used to control the size distribution of the microparticles, the thickness, and the chemical nature of the shell, which influence the release rate of the active substance [17]. The chemical and thermal characteristics of microparticles were studied by Fourier transform-infrared spectroscopy (FT-IR), contact angle measurement, differential scanning calorimetry (DSC), and thermogravometric analysis (TGA) to determine the influence of synthesis parameters. Furthermore, the water retention properties were discussed based on TGA and hygroscopic analysis.

2 Experimental

2.1 Preparation of Microparticles

2.1.1 Materials

Xylitol (Roquette Frères, content >99 %) ($C_5H_{12}O_5$), a polyhydric alcohol was employed as the core material and used as a shell-forming monomer. Diphenyl methylene diisocyanate (MDI) (Suprasec 2030, Hüntsman ICI; blend of MDI isomers, 4,4′-diphenyl methylene diisocyanate principally) used as second shell-forming monomers was obtained from Aldrich and Huntsman ICI. Non-ionic surfactant, Span® 85 (sorbitan trioleate), and poly(ethylene glycol)dioleate (PEG 400 dioleate) were purchased from Aldrich, and used as an emulsifier. Toluene was of reagent grade and used without further purification.

2.1.2 Preparation of Microparticles

The preparation of microparticles containing xylitol was carried out in a 250 mL of three neck round-bottomed flask equipped with a mechanical stirrer via interfacial polymerization, according to the following method. 60 mL of an aqueous solution containing 70 mass% of xylitol previously solubilized in water at 80 °C was emulsified in 120 mL of an organic phase containing toluene and 4 mass% of a binary mixture of PEG 400 dioleate and Span® 85 at 13,500 rpm with a homogenizer (ultra turrax®, Ika, Germany). After 25 min, when the expected droplet size of the emulsion was reached, the polymerization reaction was carried out by drop-wise addition of a solution containing either 48 mass% or 55 mass% of MDI in 20 mL of toluene, labeled S1 and S2, respectively (Table 1). The mixture was stirred continuously using a blade stirrer at 500 rpm at 80 °C to complete the formation of the cross-linked polyurethane shell over a 3-hour period. The resultant microparticles were recovered by filtration and washed once with toluene to remove the remaining MDI, and twice with water, and then dried at 60 °C overnight.

The encapsulation yield was calculated as the ratio of the recovered mass of microparticles and the mass of monomers and water introduced. It can be expressed as follows:

Table 1 Chemical composition, yield, and mean diameter of various microparticles used in this study

Samples	MDI (mass%)	Yield (%)	Mean diameter (μm)
S1	48.0	85.5	15.3 ± 1.9
S2	55.0	59.1	17.4 ± 0.8

$$\eta\,(\%) = \frac{m_{\text{microparticles}}}{\sum m_{\text{monomers,water}}} \times 100 \tag{1}$$

2.2 Characterization

2.2.1 Physicochemical Microparticle Characterization

2.2.1.1 Optical Microscopy At least 200 microparticles were picked up from the photographs of an optical microscope (OM, Axiolab Polar Carl Zeiss) using a ×40 objective lens, and the diameters were measured to obtain the number average diameter of the microparticles. The photographs were captured using the Perfect Image-Vision Clara. Three points in the circular shape of each particle observed were pointed to obtain the mean diameter.

2.2.1.2 Infrared Spectra Analysis The chemical structure of the samples was analyzed by infrared spectra in an absorbance mode, and recorded using Nicolet Nexus, connected to a PC, in which the number of scans was 256 and the resolution was $0.5\,\text{cm}^{-1}$. Samples were ground and mixed with KBr to make pellets.

2.2.1.3 Surface Hydrophobicity and Wettability of microparticles were evaluated by contact angle measurements using a contact angle meter (Digidrop, GBX, France), equipped with a diffuse light source, a CCD camera (25 fps). The contact angles (θ) are measured by three reference liquids, i.e., water, diiodomethane, and α-bromonaphtalen against a disk (10^9 Pa, 14 mm in diameter) of microparticles obtained by compression at room temperature of the powder. A droplet of liquid is placed on a pellet, and the image is immediately sent via the camera to the computer for analysis. The volume of a single droplet is about 6 μL. The polar and dispersive contributions to the surface tension of microparticles were calculated according to the method of Owens and Wendt [18] with water, α-bromonaphtalen, and diiodomethane. Constant values for the test liquids used for contact angle measurements are shown in Table 2 [19].

Each surface was measured with five independent drops of the three reference liquids, allowing us to distinguish independently the dispersed and the non-dispersed

Table 2 Surface-tension parameters of probe liquids

Probe liquids	γ_l (mJ · m^{-2})	γ_{ld} (mJ · m^{-2})	γ_{lp} (mJ · m^{-2})
Water	72.8	21.8	51.0
Diiodomethane	50.8	48.5	2.3
α-Bromonaphtalene	44.6	44.6	0.0

components of each material. No significant variations were found within any single surface. Drops were always placed at least 10 mm apart and never closer that 10 mm to an edge.

2.2.2 Thermal Analysis

2.2.2.1 Differential Scanning Calorimetry The thermal behavior of the particles was recorded using a TA instrument type DSC 2920 piloted on PC with TA Advantage control software. Indium was used as a standard for temperature calibration and the analysis was made under a constant stream of nitrogen ($50\,\mathrm{mL}\cdot\mathrm{min}^{-1}$). Samples were placed in aluminum pans which were hermetically sealed before being placed on the calorimeter thermocouples. The sample space was purged with nitrogen at a constant flow ($50\,\mathrm{mL}\cdot\mathrm{min}^{-1}$) during the experiments and the temperature range was from $-30\,^{\circ}\mathrm{C}$ to $150\,^{\circ}\mathrm{C}$. Transition temperatures and enthalpies were obtained by averaging the results of a series of four independent experiments on (5.0 ± 0.2) mg samples with at scanning speed of $1\,\mathrm{K}\cdot\mathrm{min}^{-1}$.

The content of xylitol in the microparticles can be estimated according to the measured enthalpy:

$$\text{xylitol content} = \frac{\Delta H_{\text{microparticles}}}{\Delta H^{0}_{\text{xylitol}}} \times 100\ \% \tag{2}$$

where $\Delta H_{\text{microparticles}}$ and $\Delta H^{0}_{\text{xylitol}}$ are the melting enthalpy of microparticles and xylitol, respectively.

2.2.2.2 Thermogravimetric Analyses were realized to characterize either the thermal stability or the water release profile of microparticles (cf. "Water Retention Properties").

- Thermal stability/degradation

Thermogravimetric measurements were carried out using TGA 2950 from TA Instruments at a constant heating rate of $10\,^{\circ}\mathrm{C}\cdot\mathrm{min}^{-1}$ under high purity nitrogen (99.999 %) with a flow rate of $60\,\mathrm{mL}\cdot\mathrm{min}^{-1}$. The mass of the samples used was kept between 15 mg and 16 mg in an open platinum pan. The temperature range was from ambient temperature to $650\,^{\circ}\mathrm{C}$.

2.2.3 Water Retention Properties

2.2.3.1 Hydrous Characterizations consisted of measuring the relative mass uptake of water ($\mathrm{m}\%_{\mathrm{H_2O}}$) in a controlled atmosphere (CLIMATS-2221-HA) at various relative humidities (RH) (from 50 % to 100 %) at $20\,^{\circ}\mathrm{C}$ and $35\,^{\circ}\mathrm{C}$, as follows:

$$m\,\%_{\mathrm{H_2O}} = 100\frac{m_{\mathrm{H_2O}}}{m_0} \tag{3}$$

where $m_{\mathrm{H_2O}}$ and m_0 are, respectively, the mass of adsorbed water and the initial mass of either xylitol in the microparticles or raw xylitol.

2.2.3.2 The Enthalpies of Dilution were determined with an isothermal calorimeter Setaram C80, equipped with a reversible mixing cell. A determined mass (m_s) of raw xylitol (or S1, S2) was introduced in the bottom part of the mixing cell closed by a stopper, and a mass of distilled water (m_w, $m_w = m_s$ for xylitol sample, and $m_w = m_s/2$ for S1 and S2) was then added. A mass ($m_s + m_w$) of water was introduced in the reference cell. The two cells were introduced into the calorimeter, and when the base line was stable, data acquisition was started for 3 h. After approximately 12 min, C80 was mechanically turned over ten times to mix water and the powder at 35 °C.

2.2.3.3 Moisture Retention Properties TGA was used to assess the sample moisture and water release during the temperature scan. The instrument used was a Netzsch STA 449C. Measurements were performed on raw xylitol, and S1 and S2 microparticles, exposed to water vapor in a climatic chamber (25 °C; 90 %-RH) during 4 h beforehand. In this stuy, three heating rates (0.1 $K \cdot min^{-1}$, 1 $K \cdot min^{-1}$, and 5 $K \cdot min^{-1}$) were used to evaluate the water release rate in the 25 °C to 35 °C temperature range. In these experiments, air atmosphere was used at a flow rate of 60 $mL \cdot min^{-1}$, at 35 °C (isotherm) for 100 min.

3 Results and Discussion

3.1 Formation and Structure of the Microparticles

The interfacial polymerization system has been successfully employed to encapsulate water-soluble core materials. The core substance dispersed in the organic phase is entrapped by shell material in the dispersed phase, and then the hardened microparticles can be obtained after complete polycondensation of MDI with xylitol. Figure 1 shows an optical photograph of microparticles S1 and S2 produced with 48 mass% and 55 mass% of MDI, respectively. As shown in Fig. 1, the encapsulation of xylitol is successfully carried out and the microparticles have stable and ovoidal forms. The MDI amount introduced has a low effect on the size of the microparticles. It was found that the mean diameters are about 15 μm and 17 μm for S1 and S2, respectively. Nevertheless, the most important factor in determining the final size was the concentration of MDI. Thus, this difference should be attributed to an increase of viscosity in the continuous phase by increasing the MDI amount. Figure 1 (S1-B and S2-B) compares micrographs of microparticles at a magnification of 40. Distinct core and shell domains are visible in both the S1 and the S2 microparticles. The core microparticles seem to contain submicronic dispersed particles of xylitol. The use of 48 mass% of MDI (S1 microparticles) provided a better physical aspect to the dried microparticles and hindered their aggregation. Furthermore, an increase of MDI content does not improve the encapsulation yield (Table 1) and the shape of the microparticles seems to be deformed. Based on these findings, crystallization of xylitol was initiated during the microencapsulation process by the evacuation of the water in the inner aqueous phase. Therefore, the resulting porous microparticles exhibited a web-like or hollow interior.

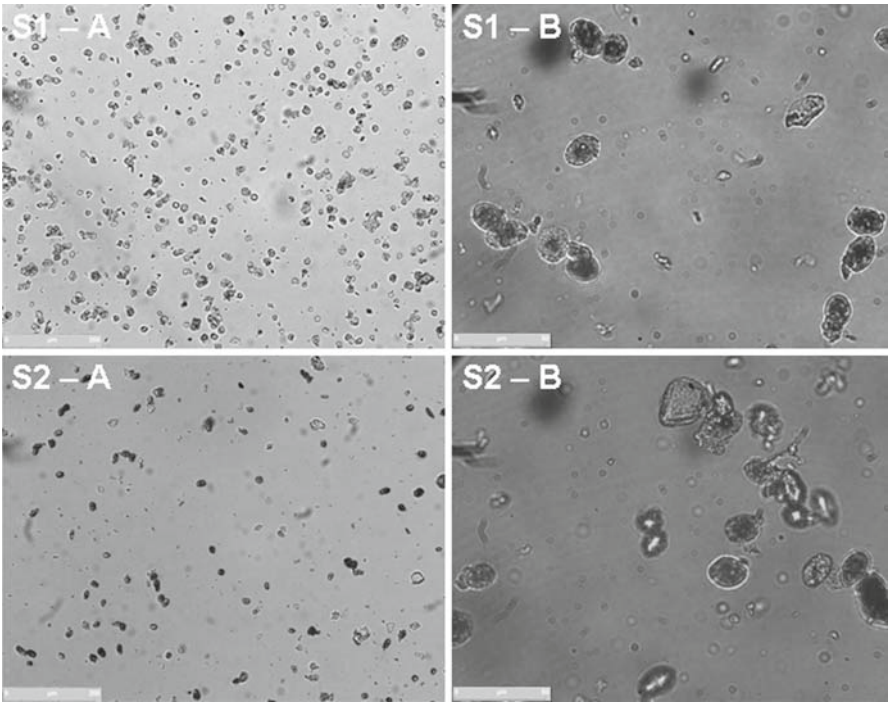

Fig. 1 Optical microscopy observation of S1 and S2 in paraffin at ×10 (S1-A and S2-A) and ×40 (S1-B and S2-B) magnification

FT-IR spectra in the transmittance mode of Xylitol, MDI, and microparticles (S1 and S2) are depicted in Fig. 2 to allow for identification of various core and shell microparticles via known characteristic wavenumbers. For polyurethane or polyurea networks prepared from isocyanate and diols, the reaction of isocyanate groups with water molecules was promoted during the shell formation process that also forms urea cross-links. The following groups are relevant to the investigations reported here: OH (broad band at 3500 cm^{-1}), isocyanate [(2280 to 2270) cm^{-1}], urea (1670 cm^{-1}), and urethane (1705 cm^{-1}). As seen in Fig. 2, the S1 and S2 spectra exhibits absorption bands at (1740 to 1700) cm^{-1} for the C=O stretching of urethane and at (1710 to 1650) cm^{-1} for urethane–urea formation. N–H stretching is evidenced with a broad-band lying in the (3450 to 3300) cm^{-1} range. In the stretching mode region of the water molecules, three overlapped bands appear between 3500 cm^{-1} and 3100 cm^{-1}. The C–H asymmetrical and symmetrical stretchings due to the methyl and methylene groups are observed between 2920 cm^{-1} and 2870 cm^{-1}. The appearance of C–O–C stretching at 1130 cm^{-1}, and =C–H bending at 820 cm^{-1} are also observed. N–H bending and C–N stretching at 1536 cm^{-1} and 1250 cm^{-1} are also observed. FT-IR spectra of microparticles also contain characteristic bands of MDI at (1600, 1410, and 820) cm^{-1} assigned, respectively, to C=C stretching, C–C stretching, and C–H bending in aromatic groups. Furthermore, the spectra S1 and S2 clearly show that xylitol was successfully microencapsulated, as it results from the presence of characteristic absorption

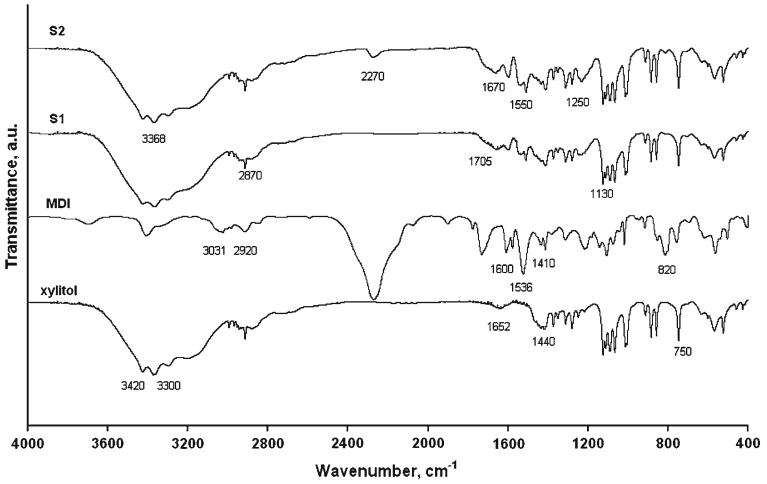

Fig. 2 FT-IR spectra of MDI, xylitol, S1 and S2 microparticles

bands of water (or hydroxyl) stretching vibrations at (3420, 3368, and 3300) cm^{-1} and in the region of (900 to 850) cm^{-1} for the CH_2 rocking band of the xylitol backbone. The completion of polycondensation reaction between MDI and xylitol was confirmed by FT-IR analysis of S1 with the absence of an absorption band due to isocyanate groups (2270 cm^{-1}), while the S2 spectrum presents this band. Thus, the microparticles from the S2 batch contain in their inner core some isocyanate groups.

To further investigate the influence of the feed ratio on the microparticle chemical structure, contact angle measurements were monitored. The measurement of the contact angle is well known and a very useful technique to examine the hydrophilic–hydrophobic properties. Table 3 shows the contact angles (θ) of the microparticles using three probe liquids. The wetting liquids with higher surface tensions have smaller contact angles toward the solid surfaces. The contact angles of the microparticles with water are decreased, and the contact angles of the microparticles with α-bromonaphtalen are increased as the MDI amount introduced increased. The surface free energy factor calculated from the method of Owens and Wendt [18] are also shown in Table 3. Thus, xylitol showed a higher polar component than those of S1 and S2, while dispersive components are close to each other. These results should be explained by the effect of polar groups on the surface (i.e., hydroxyl group for xylitol) which is bigger than that of the dispersive force. Furthermore, the surface free energy of both microparticles is lower than xylitol, but increases with an increase in the MDI amount introduced. As an experimental result, those can be seen that the specific component of the surface free energy, γ_{SP}, and the hydophilicity increase with increasing MDI ratio. Whereas, no difference for the London dispersive component, γ_{Sd}, is observed. This result indicates that the increase of the MDI ratio leads to an increase of the surface free energy, γ_S, and hydrophilicity which is mainly influenced by its specific component. The entrapment of xylitol by a polyurethane shell allows modification of hydrophilicity.

Table 3 Measured contact angle of the probe liquids and calculated surface tensions by the Owens-Wendt method

Samples	Mean contact angle (θ) (°)			Surface tension[a] ($mN \cdot m^{-1}$)		
	Water	Diiodomethane	α-Bromonapthalene	γ_S	γ_{Sd}	γ_{Sp}
Xylitol	7.0 ± 2.0	32.1 ± 2.3	22.6 ± 10.6	77.1 ± 1.2	$43.1 \pm 1{,}1$	34.0 ± 0.6
S1	57.1 ± 4.9	39.7 ± 1.7	14.3 ± 2.5	58.6 ± 2.2	41.9 ± 0.6	13.0 ± 2.5
S2	51.1 ± 2.7	38.2 ± 3.1	19.5 ± 3.0	54.9 ± 3.1	42.2 ± 1.1	16.4 ± 1.1

[a] γ_S = total surface energy of the surface, γ_{Sd} = dispersive component of solid surface, γ_{Sp} = polar component of solid surface

3.2 Thermal Properties of Microparticles

By changing the ratio of the mass of the core material to that of the coating material, a microencapsulated form-stable xylitol in different proportions is prepared. Its thermal properties such as phase change enthalpy, phase change temperature, and glass transition temperature are measured using a DSC instrument, and the results are shown in Table 4. DSC analyses of raw xylitol, and S1 and S2 samples, resulted in well-performed endothermic enthalpy changes during heating between $-30\,°C$ and $150\,°C$. From the DSC curve of the raw xylitol in Fig. 3, a sharply endothermic peak corresponding to the melting process was observed at $93.71\,°C$ with an enthalpy of $248.7\,J \cdot g^{-1}$ which is in accordance with those reported in the literature [20–25]. The glass transition temperature (T_g) determined from the second run (Fig. 3) was found at $-24.04\,°C$. The glass transition was followed by a exothermic crystallization occurring over a temperature range from $-10\,°C$ to $5\,°C$. In S1 and S2 samples, the phase transition interval coincides with that of raw xylitol but the enthalpy changes observed are distinctive. Shifts of the melting temperature can be attributed to the low thermal conductivity of the polymer shell and to the crystalline xylitol content (Table 4). The percentage of crystalline xylitol in microencapsulated materials is the key factor for humidity sensor microparticles. The enthalpies of the dried microparticles S1 and S2 are, respectively, $158.6\,J \cdot g^{-1}$ and $131.3\,J \cdot g^{-1}$; thus, the microparticles contain 63.8 mass% and 52.8 mass% of crystalline xylitol, respectively. These values are slightly lower than the theoretical content, which indicates that 7 mass% of xylitol was reacted with MDI to produce a polymer shell. The glass transition temperatures are shifted to a lower temperature due to a plasticization effect by the residual water

Table 4 Thermal properties of xylitol and microparticles in this study

Sample	Enthalpy of fusion ($J \cdot g^{-1}$)	Crystalline xylitol content (mass%)	T_g (°C)	T_m (°C)	T_m/T_g	Enthalpy of dissolution ($J \cdot g^{-1}$)
Xylitol	248.7	100	−24.04	93.71	1.47	167.07
S1	158.6	63.8	−27.01	95.60	1.50	127.94
S2	131.3	52.8	−26.20	96.70	1.50	38.14

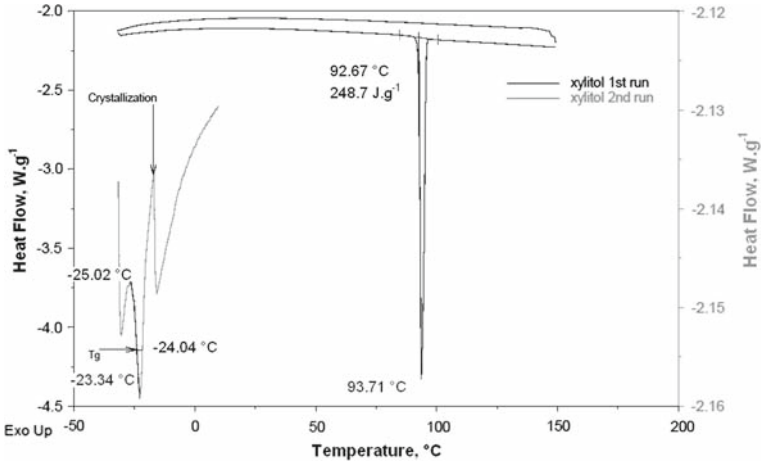

Fig. 3 DSC curve of xylitol (N_2, $1\,K \cdot min^{-1}$)

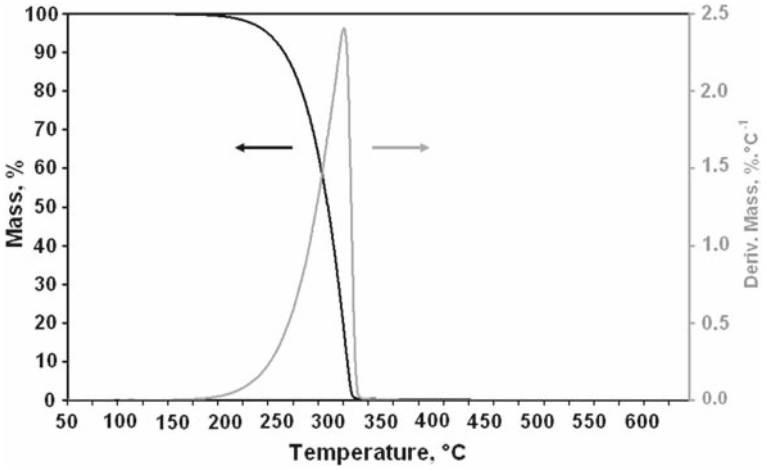

Fig. 4 TG and DTG curves of xylitol

molecule. Furthermore, the crystallization of xylitol was not observed on the DSC trace. The tendency of polyols to crystallize can be estimated by the ratio of T_m and T_g (T_m/T_g). The encapsulation step allows an increase of this ratio from 1.47 to 1.5. However, no exothermic peak was detected by DSC with a cooling rate of $1\,K \cdot min^{-1}$. Nevertheless, a new endothermic peak was observed after a time lag of about 12 h at room temperature.

From the TG curve (Fig. 4), it can be seen that the mass loss of sample was completed in a single step. The sample keeps thermostable below 180 °C. It begins to lose mass at 200 °C, reaches the maximum rate of mass loss at 324 °C, and completely loses mass when the temperature reaches 332 °C. Similar results were obtained by Tong et

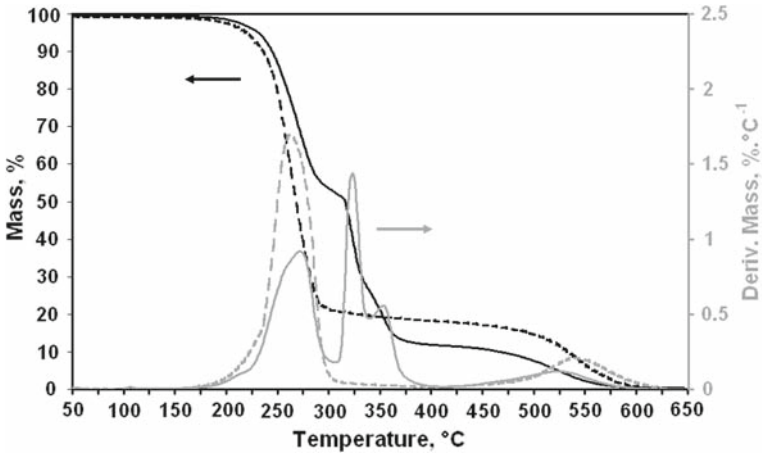

Fig. 5 TG (▬) and DTG (▬) curves of S1 (▬) and S2 (▬ ▬ ▬) microparticles

al. [20]. The TG and DTG curves of S1 and S2 are shown in Fig. 5. The mass loss was completed in 3 and 2 steps for S1 and S2, respectively. Thus, from 280 °C, the degradation and the depolymerization of polyurethane polymer and oligomers were observed. This step was followed by a recombination in urea oligomers, which were degraded at a higher temperature. The main steps of degradation of microparticles containing xylitol occur between 200 °C and 400 °C. Sample S2 shows one peak between 200 °C and 300 °C with 75 % mass loss, whereas sample S1 shows one peak between 200 °C and 300 °C and two overlapping peaks between 300 °C and 400 °C corresponding to a mass loss of 85 %. Comparatively, the mass loss temperature of microparticles is higher than that of the raw xylitol. Furthermore, the thermal stability of S1 from 200 °C to 320 °C was higher than that of S2. Thus, the mole ratio of MDI and xylitol in the polymer shell has effects on the thermal stability of the microparticles.

The previous results also indicate that the morphology of the microparticles should be different according to the MDI amount introduced. Thus, during the formation of the shell, MDI, water, and xylitol are mixed together to form oligomers and to create an interpenetrated network. On the one hand, if the oligomers formed are soluble in the droplet phase, they lead to the formation of a matricial structure. On the other hand, when they are insoluble in the droplets, they collapse at the interface, and a capsular structure can be obtained. In our study, the MDI amount introduced changes in the solubility parameters of the medium, which leads to the formation of a matricial structure (S2) more homogenous than the capsular structure (S1).

3.3 Water Retention Properties

The hygroscopicity of xylitol and microencapsulated xylitol is shown in Fig. 6. The three samples had the same critical relative humidity (CRH) at 20 °C (70 % RH), whereas the CRH were 60 % RH for S1 and S2 and less than 50 % RH for xylitol. Thus, the microencapsulation allows reduction of the hygroscopicity of xylitol.

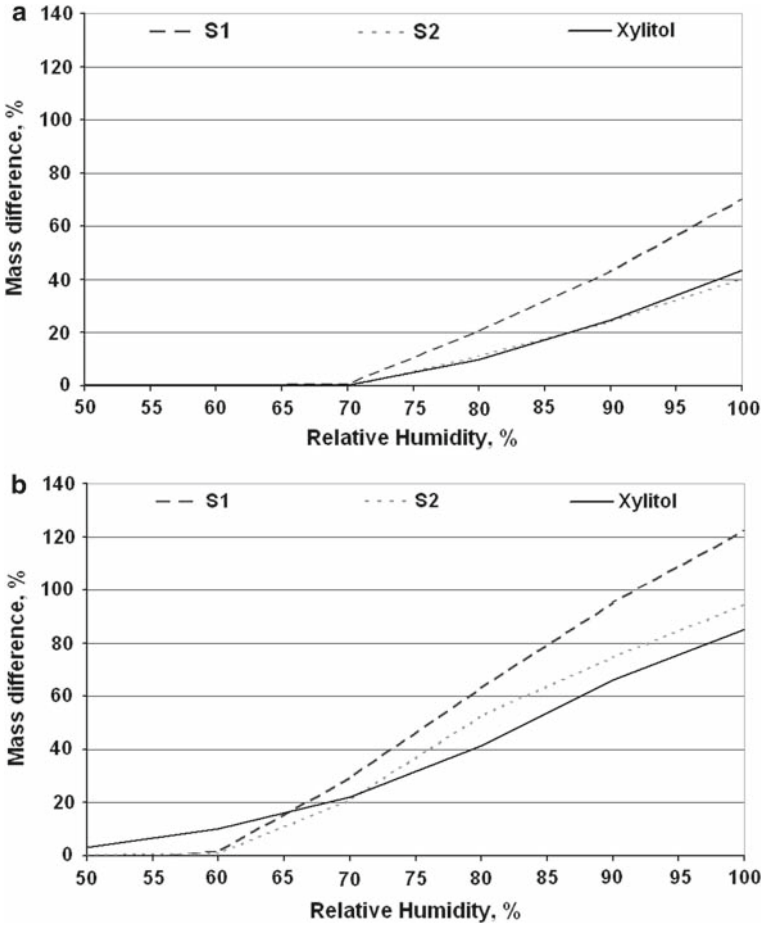

Fig. 6 Hygroscopicity at (**a**) 20 °C and (**b**) 35 °C of xylitol, S1 and S2 microparticles

Heats of dilution of xylitol, S1, and S2 were measured at 313 K in water and are reported in Table 4. For the investigated systems, dilution is an endothermic process. Xylitol forms strong hydrogen bonds with one another and with water, which leads to a higher order structure. Xylitol has an enthalpy of dilution of 167 $J \cdot g^{-1}$. Moreover, it was observed that the enthalpy of dilution of S1 (127.9 $J \cdot g^{-1}$) was higher than that of S2 (38.1 $J \cdot g^{-1}$). The value obtained for S2 was very low in relation to the crystalline xylitol content. Thus, the matricial structure was not suitable to diffuse liquid water to xylitol; therefore, the polymer network acted as a barrier and solubilization of xylitol was incomplete. The S1 value was higher than expected and was due to the ability of the free hydroxyl group of the polymer shell to create hydrogen bonds with water. Thus, the enthalpy of dilution was affected by the morphology of the microparticles.

The water released from xylitol and microparticles was determined by TGA (Figs. 7, 8, 9, and 10). The various figures show the influence of temperature programs on the water released. The heating rate influences the water release; thus, the higher is the

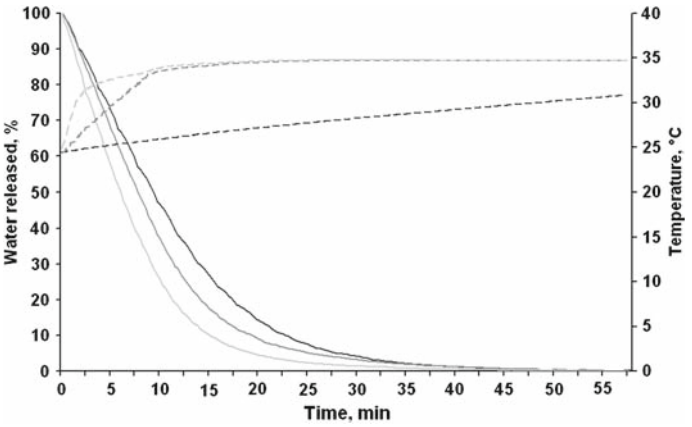

Fig. 7 Influence of the temperature programs on water released from S2 [1st temperature program (▬), 2nd temperature program (▬) and 3rd temperature program (▬)] and temperature vs. time at 0.1 K · min^{-1} (1st temperature program, ▬ ▬ ▬); 1 K · min^{-1} (2nd temperature program, ▬ ▬ ▬); and 5 K · min^{-1} (3rd temperature program, ▬ ▬ ▬)

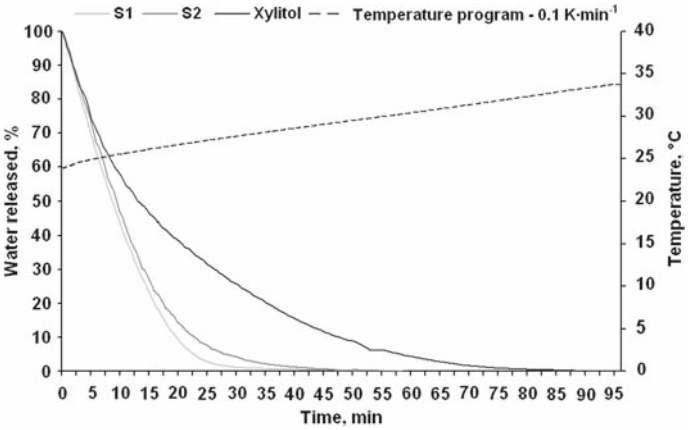

Fig. 8 Water release profile of xylitol, S1 and S2 microparticles at 0.1 K · min^{-1}

rate, the faster is the water released (Fig. 7). Nevertheless, in this temperature range, our previous attempts have shown that this influence was negligible for a heating rate above 5 K · min^{-1}. Furthermore, the rate of water release for S2 was twice as high as with a heating rate of 5 K · min^{-1} than that at 1 K · min^{-1}, which is twice as high as the third one.

Whatever the heating rate or the temperature programs applied (Figs. 8, 9, and 10), xylitol was always the compound with the lowest diffusion rate. The lower the heating rate is, the higher is the difference with the microparticles. Furthermore, we can see that S1 releases water faster than S2. From these observations, we can attribute these differences to the morphology and the surface state of the various compounds. The porosity and the roughness of the microparticles improve the water transfer and

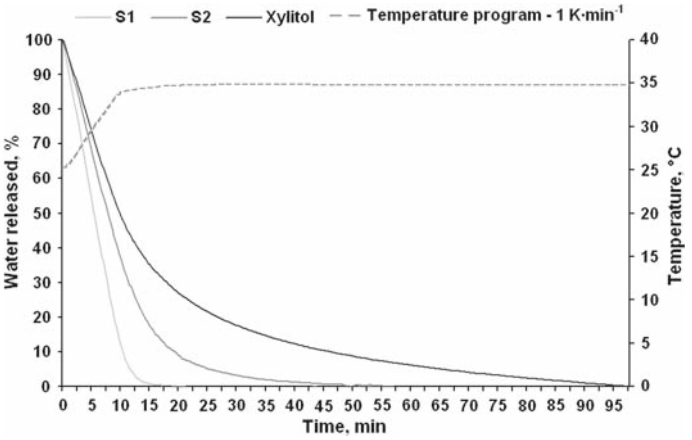

Fig. 9 Water release profile of xylitol, S1 and S2 microparticles at $1\ \mathrm{K} \cdot \mathrm{min}^{-1}$

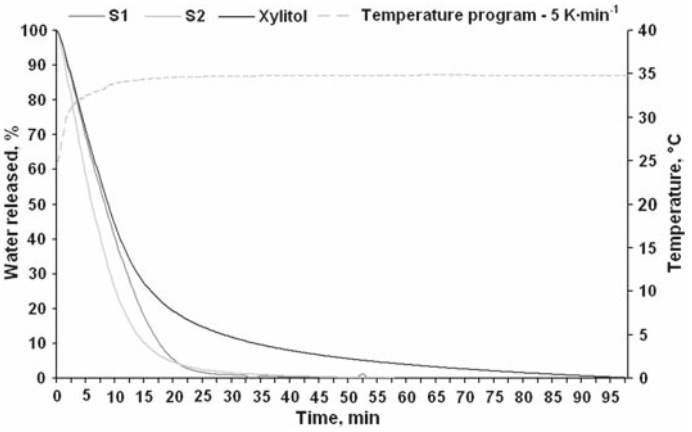

Fig. 10 Water release profile of xylitol, S1 and S2 microparticles at $5\ \mathrm{K} \cdot \mathrm{min}^{-1}$

obviously the vapor creation. The diffusion rate of S2 and xylitol can be attributed to the labyrinth effect of the xylitol crystals dispersed in the compounds and, in this way, we have a retardant release effect.

4 Conclusion

The microencapsulation of xylitol by a polyurethane–urea shell using an interfacial polycondensation method was achieved successfully. The synthesis conditions influence not only the morphology of the particles but also the loading content of crystalline xylitol. The chemical and thermal analyses of the microparticles have shown that two types of microparticles were obtained according to the MDI amount introduced, i.e., a core/shell structure (S1) with a high loading content and a matricial structure (S2) having lower thermal properties than S1. Furthermore, from the water retention

analysis, the microparticles absorb more water which is in a liquid or gas state than xylitol under the crystal form used. Water diffusion from microparticles and xylitol depends on the heating rate and the temperature. From TGA analysis, it was noted that higher release rates were found for microparticles than for pure xylitol. It was concluded that microparticles containing solid crystalline xylitol exhibits characteristics of a sweat sensor during their charge with moisture and could be interpreted due to the solubility of xylitol in water. The batch S1 has shown the best moisture transfer and cooling effect properties. Thus, the homogeneous, rough, non-aggregated, regular structure obtained improves moisture transfer. Therefore, the synthesized microparticles would be expected to be a thermal sensor to provide a cooling effect.

References

1. P. Zhang, Y. Watanabe, S.H. Kim, H. Tokura, R.H. Gong, J. Text. Ins. **92**, 372 (2001)
2. A. Weber, P. Olson, M. Long, United States Patent 7250548 (2007)
3. S. Ohmori, Y. Ohno, T. Makino, T. Kashihara, Int. J. Pharm. **278**, 447 (2004)
4. Y.G. Bryant, D.P. Colvin, United States Patent 4756985 (1988)
5. P. Colvin, Y.G. Bryant, United States Patent 5415222 (1995)
6. K.E. Kaska, M.M. Chen, J. Sol. Energy Eng. **107**, 229 (1985)
7. X. Zhang, in *Smart Fibres, Fabrics and Clothing*, ed. by X. Tao (Woodhead Limited Cambridge, 2000), pp. 34–41
8. S.K. Yadav, A.K. Suresh, K.C. Khilar, AIChE J. **36**, 431 (1990)
9. F. Salaun, E. Devaux, S. Bourbigot, P. Rumeau, Carbohydr. Polym. **73**, 23 (2008)
10. S. Canbazoğlu, A. Şahinaslan, A. Ekmekyapar, Y.G. Aksoy, F. Akarsu, Energy Build. **37**, 235 (2005)
11. K. Hong, S. Park, Polym. Test. **19**, 975 (2000)
12. K. Hong, S. Park, React. Funct. Polym. **42**, 193 (1999)
13. J.-F. Su, L.-X. Wang, L. Ren, Colloids Surf. A **299**, 268 (2007)
14. D. Saihi, I. Vroman, S. Giraud, S. Bourbigot, React. Funct. Polym. **66**, 1118 (2006)
15. D. Saihi, I. Vroman, S. Giraud, S. Bourbigot, React. Funct. Polym. **64**, 127 (2005)
16. A.M. Pensé, C. Vauthier, J.P. Benoit, Colloid Polym. Sci. **272**, 211 (1994)
17. L.J.J.M. Janssen, A. Boersma, K. te Nijenhuis, J. Membr. Sci. **79**, 11 (1993)
18. D.K. Owens, R.C. Wendt, J. Appl. Polym. Sci. **13**, 1741 (1969)
19. F.M. Fowkes, Ind. Eng. Chem. **56**, 40 (1964)
20. B. Tong, Z.-C. Tan, Q. Shi, Y.-S. Li, D.-T. Yue, S.-X. Wang, Thermochim. Acta **457**, 20 (2007)
21. G. Barone, G.D. Gatta, D. Ferro, V.J. Piancete, Chem. Soc. Faraday Trans. **86**, 75 (1990)
22. H.P. Diogo, S. Pinto, J.J. Moura Ramos, Carbohydr. Res. **342**, 961 (2007)
23. Y. Roos, Carbohydr. Res. **238**, 39 (1993)
24. L. Carpentier, S. Desprez, M.J. Descamps, J. Therm. Anal. Calorim. **73**, 577 (2003)
25. R.A. Talja, Y.H. Roos, Thermochim. Acta **380**, 109 (2001)